Design of a half-ring plasmonic tweezers for environmental monitoring

Mario Christian Falconi, Giovanni Magno, Santina Colosimo, Vy Yam, Beatrice Dagens, Francesco Prudenzano

Optical Materials: X 13 (2022) 100141

Contents lists available at ScienceDirect

Optical Materials: X

journal homepage: www.journals.elsevier.com/optical-materials-x

Invited Article

Design of a half-ring plasmonic tweezers for environmental monitoring

Mario Christian Falconi [a], Giovanni Magno [a], Santina Colosimo [a], Vy Yam [b], Beatrice Dagens [b], Francesco Prudenzano [a,*]

[a] Department of Electric and Information Engineering, Politecnico di Bari, 70125, Bari, Italy
[b] Université Paris-Saclay, CNRS, Centre de Nanosciences et de Nanotechnologies, 91120, Palaiseau, France

ARTICLE INFO

Keywords:
Gold
Half-ring
Optical trapping
Silicon-on-insulator
Tweezers

ABSTRACT

An integrated near-field plasmonic tweezers, based on two gold half-ring elements, is proposed. The device consists of a silicon-on-insulator (SOI) waveguide on which two symmetric half-ring-shaped elements are deposited. The SOI waveguide, having dimensions 500 × 220 nm, enables single mode light propagation at 1.55 μm. The structure of the half-ring plasmonic tweezers exhibits up to five design parameters: inner radius r_i, outer radius r_e, gap g, height h and angle ϑ. Gold permittivity is modeled by means of a Drude equation. The trapping performance is investigated by evaluating the optical force exerted on a nanoparticle having a radius of 25 nm, together with the stiffness and the trapping potential. Simulation results show that stable trapping is achieved for an input power as low as 27 mW at 1.55 μm, with a stiffness of −4.06 fN mW^{-1} nm^{-1}.

1. Introduction

In recent years, the development of optical devices and systems to address environmental pollution has attracted a lot of research interest. In fact, the presence of harmful particulate matter (PM) in the atmosphere, mainly produced by industrial activities and by the combustion of fossil fuels, is a source of many serious diseases, such as lung cancer, asthma attacks, allergies, etc. Such particulate matter often occurs in the form of fine dust with diameters ranging from a few microns to a few tens of nanometers. In order to monitor the exposure to PM, it is then important to develop suitable devices capable of detecting and capturing it. For this purpose, plasmonic tweezers represent excellent candidates. They allow stable trapping of nanoparticles within very compact structures by exploiting the localized surface plasmon resonance (LSPR) [1], overcoming the diffraction limit of conventional optical tweezers. Many different structures have been proposed in literature, such as bow-tie [2], nano-taper [3], dimers [4], V-type antennas [5], nanoplate tetramers [6], hexagonal arrays of triangles [7], nanopillars [8], coaxial nanoaperture [9], nanopyramids [10], etc. Moreover, the availability of devices and systems such as spargers, bubblers and condensates, makes plasmonic tweezers suitable for monitoring not only PM dispersed in liquid media, but also PM in the atmosphere [11,12].

Lin et al. proposed a gold bowtie plasmonic tweezers coupled to a silicon nitride waveguide [2]. The system was considered immersed in water, with a polystyrene bead used as nanoparticle to be trapped. The excitation wavelength was 1.62 μm. Different gaps for the bowtie were studied, from 5 to 30 nm. The structure generated highly concentrated resonant fields, allowing for trapping nanoparticles of 20 nm diameter. When the gap was fixed at 5 nm, the maximum predicted trapping force was about 652 fN mW^{-1}. The threshold power, evaluated by means of the Ashkin criterion [13], was 10.2 mW.

In [3] a triangular-shaped nano-taper coupled to a silicon nitride waveguide having dimensions 600 × 350 nm is reported. The glass substrate was made of silicon dioxide. The chosen excitation wavelength was 1.064 μm, since silicon nitride exhibits a low optical absorption at this wavelength. The device was supposed to be immersed in water. By injecting a fundamental TM mode into the waveguide, two hybrid plasmonic modes were excited. The maximum optical intensity was obtained on the front tip of the nano-taper, inducing a strong trapping force on the nanoparticle. In order to find the best taper length, the trapping force was studied for different gold heights, from 10 to 60 nm. The optimal length identified was 625 nm, with a gold height of 20 nm. Trapping performance was evaluated for polystyrene nanoparticles of 100 nm diameter. Two different stable positions were found, one of which was near the front tip and exhibited the deepest potential well of $2.798k_BT$ mW^{-1}. Therefore, according to the Ashkin criterion, the nanoparticle could be stably trapped with a threshold power as low as 3.57 mW.

* Corresponding author.
E-mail addresses: mariochristian.falconi@poliba.it (M.C. Falconi), giovanni.magno@poliba.it (G. Magno), s.colosimo@studenti.poliba.it (S. Colosimo), vy.yam@c2n.upsaclay.fr (V. Yam), beatrice.dagens@c2n.upsaclay.fr (B. Dagens), francesco.prudenzano@poliba.it (F. Prudenzano).

https://doi.org/10.1016/j.omx.2022.100141
Received 20 November 2021; Received in revised form 27 January 2022; Accepted 29 January 2022
Available online 3 February 2022

A. Ecarnot at al. proposed a plasmonic tweezers based on gold dimers coupled to a silicon-on-insulator (SOI) waveguide [4]. The device operated in the 1.35–1.75 μm wavelength range. The dimers had an ellipsoidal shape, with radii of 40 nm (x-direction) and 100 nm (y-direction). The gold height was 30 nm. A Drude model was used to account for gold permittivity. Polystyrene beads with radii ranging from 250 to 50 nm and immersed in water were considered. LSPR excitation was demonstrated at 1.52 μm for the gap size of 20 nm, with a calculated absorbance of over 55%. The best trapping performance was obtained for nanoparticles having a radius of 50 nm, with a low threshold power of about 10 mW and a stiffness along the x-direction of −3.12 fN nm^{-1} mW^{-1}.

In this work, we propose a plasmonic tweezers based on two gold half-ring elements deposited on a silicon-on-insulator (SOI) waveguide (see Fig. 1). The SOI waveguide, having dimensions 500 × 220 nm, enables single mode light propagation at 1.55 μm. The structure of the half-ring plasmonic tweezers exhibits up to five geometrical parameters (inner radius r_i, outer radius r_e, gap g, height h and angle ϑ) providing great flexibility for the design. In particular, the proposed structure compared with [4] exhibits a higher number of degrees of freedom that can be exploited to tailor the design, in terms of both spectral properties and excitation efficiency of the nanoantenna. Firstly, the transmittance and the reflectance of the device are studied by means of a commercial finite-difference time-domain (FDTD) software and optimized to determine the geometrical parameters that allow the LSPR resonance peak to be positioned around the wavelength of 1.55 μm. Then, the optical force exerted on a polystyrene nanoparticle having a radius of 25 nm is calculated using the volumetric technique [14]. Finally, the stiffness and the trapping potential are evaluated to determine the points of stable equilibrium.

2. Design

2.1. Study of the LSPR excitation

The design of the half-ring plasmonic tweezers is performed by means of Lumerical FDTD software. The simulation approach was validated by considering the numerical and experimental results for the structure reported in Refs. [4,14]. An optimum agreement was obtained for the transmittance and reflectance spectra, and for the trapping stiffness and potential. Table 1 reports the optical parameters for all the materials used in the simulation. In particular, gold permittivity is modeled by means of the well-known Drude equation:

$$\varepsilon_r(\omega) = \varepsilon_\infty - \frac{\omega_p^2}{\omega(\omega + j\gamma)} \quad (1)$$

where j is the imaginary unit. The values for the high-frequency permittivity ε_∞, the plasma frequency ω_p and the collision frequency γ of gold are taken from the literature [4,14]. The geometrical parameters of the SOI waveguide and the nanoparticle are also reported in the same table. Perfectly matched layers (PMLs) are employed to avoid reflections into the computational domain. The optical mode injected into the SOI waveguide is the fundamental TE mode. The amplitude of the input electric field is normalized to $E_0 = 1$ V/m. Since the plasmonic tweezers exhibits a high number of design parameters, up to five, finding the right combination to ensure a good coupling between the waveguide and the half-ring elements is not trivial. Therefore, preliminary simulations are carried out by a trial-and-error approach to determine suitable nominal values for the design parameters allowing a resonance in the λ = 1.35–1.75 μm wavelength range. In this part, the nanoparticle is not considered, i.e. it is removed from the simulation. Feasible values for all the design parameters are used to make realistic a potential fabrication. In particular, the gap g has been kept always higher than 15 nm, even if with current manufacturing technologies it is possible to obtain ultrasmall gaps down to the sub-10 nm scale [15]. The identified parameters are the following: $r_i = 60$ nm, $r_e = 75$ nm, g = 20 nm, h = 15 nm, ϑ = 90°.

In order to study the behavior of the device with respect to its geometrical parameters, a number of parametric sweeps is performed by varying: i) the inner radius, ii) the outer radius, iii) the gap, iv) the height, v) the angle. The results, in terms of transmittance and reflectance spectra, are reported in Figs. 2–6. In each simulation, only one parameter is varied at a time, keeping the others fixed. The transmittance T is evaluated with a power monitor in the yz-plane put after the tweezers, while the reflectance is evaluated with another power monitor in the yz-plane put before the source injection plane.

Fig. 2 shows the transmittance T and the reflectance R as functions of the wavelength λ for different inner radii r_i. As the inner radius increases, the resonance wavelength undergoes a red shift, from λ = 1.35 μm to λ = 1.63 μm. In addition, for inner radius values greater than r_i = 62 nm, the transmittance decreases, i.e. a better absorption is obtained. Regarding the reflectance, a red shift is also observed, with very small absolute values. This confirms that the device reflects a very small power.

Fig. 3 shows the transmittance T and the reflectance R as functions of the wavelength λ for different outer radii r_e. In contrast to the previous case, increasing the outer radius produces a blue shift of the resonance wavelength from λ = 1.54 μm to λ = 1.41 μm. In addition, the transmittance varies slightly, staying around T = 0.81–0.83. Reflectance shows a similar behavior, still with very low values.

Fig. 4 shows the transmittance T and the reflectance R as functions of

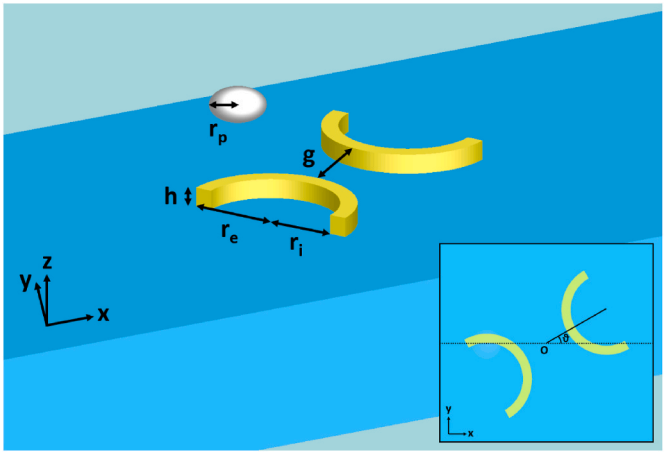

Fig. 1. 3D sketch of the proposed optical plasmonic tweezers. The half-ring elements are deposited on a silicon-on-insulator (SOI) waveguide. The five geometrical parameters of the device, i.e. the inner radius r_i, the outer radius r_e, the gap g, the height h and the angle ϑ (representing the tilt of the nanoantenna around the z axis, see the inset), are reported. The radius of the nanoparticle is denoted by r_p. The point O = (0, 0, 0) nm under the SOI waveguide core is the origin. (For interpretation of the references to colour in this figure legend, the reader is referred to the Web version of this article.)

Table 1
Optical and geometrical parameters employed in the simulation of the half-ring plasmonic tweezers.

Parameter	Symbol	Value
Silicon refractive index at 1550 nm	n_{Si}	3.48
Silicon dioxide refractive index at 1550 nm	n_{SiO2}	1.45
Water refractive index at 1550 nm	n_{water}	1.318
Nanoparticle refractive index at 1550 nm	n_{bead}	1.59
Gold high-frequency permittivity	ε_∞	1 [14]
Gold plasma frequency	ω_p	1.29×10^{16} rad/s [14]
Gold collision frequency	γ	6.478×10^{13} rad/s [14]
Silicon waveguide width	w_{Si}	500 nm
Silicon waveguide height	h_{Si}	220 nm
Nanoparticle radius	r_p	25 nm

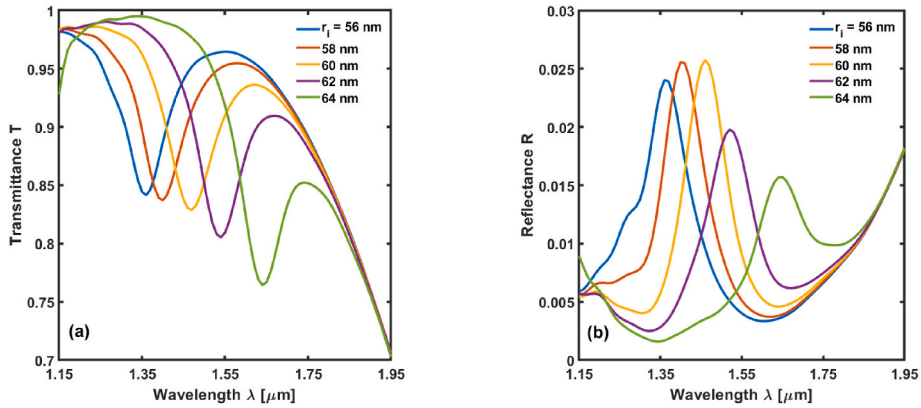

Fig. 2. (a) Transmittance T and (b) reflectance R as functions of the wavelength λ for five different inner radii, $r_i = 56$ nm (blue curve), $r_i = 58$ nm (red curve), $r_i = 60$ nm (yellow curve), $r_i = 62$ nm (purple curve), $r_i = 64$ nm (green curve). Outer radius $r_e = 75$ nm, gap g = 20 nm, height h = 15 nm, angle $\vartheta = 90°$. (For interpretation of the references to colour in this figure legend, the reader is referred to the Web version of this article.)

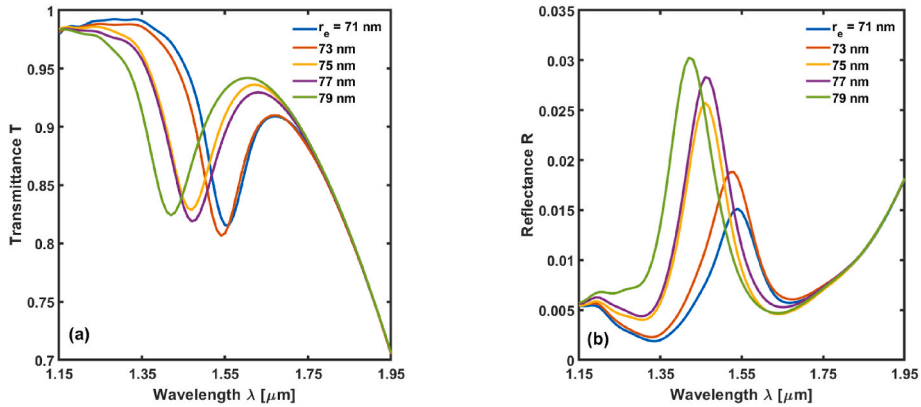

Fig. 3. (a) Transmittance T and (b) reflectance R as functions of the wavelength λ for five different outer radii, $r_e = 71$ nm (blue curve), $r_e = 73$ nm (red curve), $r_e = 75$ nm (yellow curve), $r_e = 77$ nm (purple curve), $r_e = 79$ nm (green curve). Inner radius $r_i = 60$ nm, gap g = 20 nm, height h = 15 nm, angle $\vartheta = 90°$. (For interpretation of the references to colour in this figure legend, the reader is referred to the Web version of this article.)

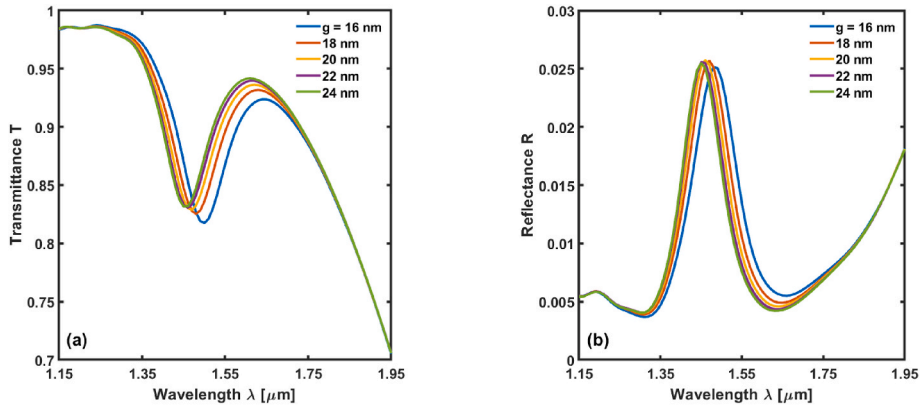

Fig. 4. (a) Transmittance T and (b) reflectance R as functions of the wavelength λ for five different gaps, g = 16 nm (blue curve), g = 18 nm (red curve), g = 20 nm (yellow curve), g = 22 nm (purple curve), g = 24 nm (green curve). Inner radius $r_i = 60$ nm, outer radius $r_e = 75$ nm, height h = 15 nm, angle $\vartheta = 90°$. (For interpretation of the references to colour in this figure legend, the reader is referred to the Web version of this article.)

the wavelength λ for different gaps g. Like the previous case, as the gap increases, the resonance wavelength decreases, but less noticeably. It is also observed that the gap has little influence on the transmittance value. A similar behavior occurs for the reflectance, which remains below R = 0.026.

Fig. 5 shows the transmittance T and the reflectance R as functions of the wavelength λ for different heights h. It is observed that the height greatly affects the resonance wavelength, which decreases from λ = 1.61 μm to λ = 1.36 μm. Also, low values of the height allow for better coupling between the waveguide and the tweezers. The reflectance continues to remain below R = 0.026.

Fig. 6 shows the transmittance T and the reflectance R as functions of the wavelength λ for different angles ϑ between the geometrical axes of the half-ring elements and the propagation direction x. It is apparent

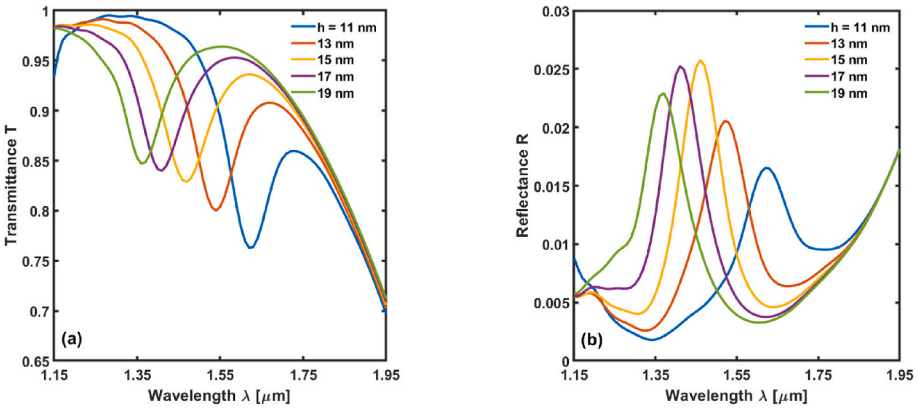

Fig. 5. (a) Transmittance T and (b) reflectance R as functions of the wavelength λ for five different heights, h = 11 nm (blue curve), h = 13 nm (red curve), h = 15 nm (yellow curve), h = 17 nm (purple curve), h = 19 nm (green curve). Inner radius r_i = 60 nm, outer radius r_e = 75 nm, gap g = 20 nm, angle ϑ = 90°. (For interpretation of the references to colour in this figure legend, the reader is referred to the Web version of this article.)

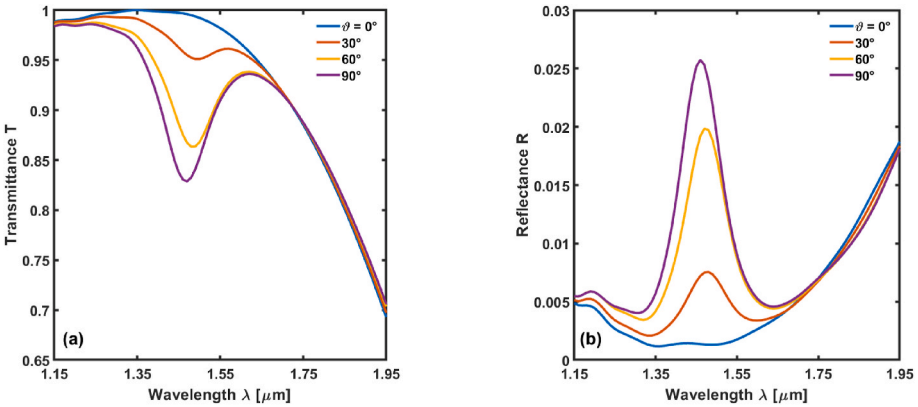

Fig. 6. (a) Transmittance T and (b) reflectance R as functions of the wavelength λ for five different angles, ϑ = 0° (blue curve), ϑ = 30° (red curve), ϑ = 60° (yellow curve), ϑ = 90° (purple curve). Inner radius r_i = 60 nm, outer radius r_e = 75 nm, gap g = 20 nm, height h = 15 nm. (For interpretation of the references to colour in this figure legend, the reader is referred to the Web version of this article.)

that the resonance wavelength is almost insensitive to the rotation of the structure. The largest difference is observed for the transmittance intensity, which decreases as the angle increases. This result suggests that the coupling between the waveguide and the tweezers is maximum when the half-ring elements are parallel to the propagation direction, i.e. ϑ = 90°. In other words, the maximum coupling is obtained when the center-to-center axis of the half-ring elements is aligned with the injected electric field, which is polarized along the y-direction. The reflectance shows an identical behavior.

By exploiting the results obtained from the parametric sweeps, the following values for the design parameters are chosen: inner radius r_i = 60 nm, outer radius r_e = 71 nm, gap g = 20 nm, height h = 15 nm, angle ϑ = 90°.

2.2. Evaluation of the optical trapping force

In order to investigate the trapping performance of the proposed plasmonic tweezers, the nanoparticle is added to the model and the optical force exerted on it is evaluated by means of the volumetric technique [14]. The position of the nanoparticle is varied along both the x-direction (i.e. with y_p = 0 nm) and the y-direction (i.e. with x_p = 0 nm). It is worth pointing out that the nanoparticle is put in contact with the half-ring elements along the z-direction, i.e. at $z = h_{Si} + h + r_p$ (see Fig. 1). Surface roughness is not considered in the model since its contribution can be neglected provided that the ratio between the correlation length and the root mean square (RMS) height is high enough, larger than 10 [16]. Thermal effects were not taken into account in this study since the photothermal effect can be mitigated by exploiting heat sinks or by decreasing the power density among the plasmonic nanostructures [17].

Fig. 7(a) shows the x-component F_x of the optical force as a function of the nanoparticle position x_p and the wavelength λ. At the wavelength λ = 1.55 μm, the nanoparticle is affected by the force exerted by the plasmonic tweezers mainly within a range of $x_p = \pm 50$ nm with respect to the center of the structure, i.e. x_p = 0 nm, at which point the force changes sign (from positive to negative). A similar behavior is observed in Fig. 7(b), which shows the y-component F_y of the optical force as a function of the nanoparticle position y_p and the wavelength λ. The presence of two sign inversions from positive to negative for the optical force F_y depends on the fact that the nanoparticle, moving along the y-axis, encounters two distinct gold-water interfaces at $y_p = \pm g/2$. This effect is more apparent for small nanoparticles [4]. Moreover, the z-component of the optical force, calculated in (x_p, y_p) = (0, 0) nm, is equal to $F_z = -301.3$ fN mW^{-1}, i.e. the nanoparticle is pushed towards the tweezers along the z-direction. This suggests that (x_p, y_p) = (0, 0) nm is an equilibrium position for the nanoparticle.

In order to assess the trapping stability, the stiffness and also the trapping potential need to be evaluated. In fact, equilibrium is stable only if the Ashkin criterion [13] is met, i.e. if the trapping potential U depth is at least equal to $10k_BT$, where k_B is the Boltzmann constant and T = 298 K is the temperature of the system. The stiffness is defined as the spatial derivative of the optical force, while the trapping potential is given by the following integral:

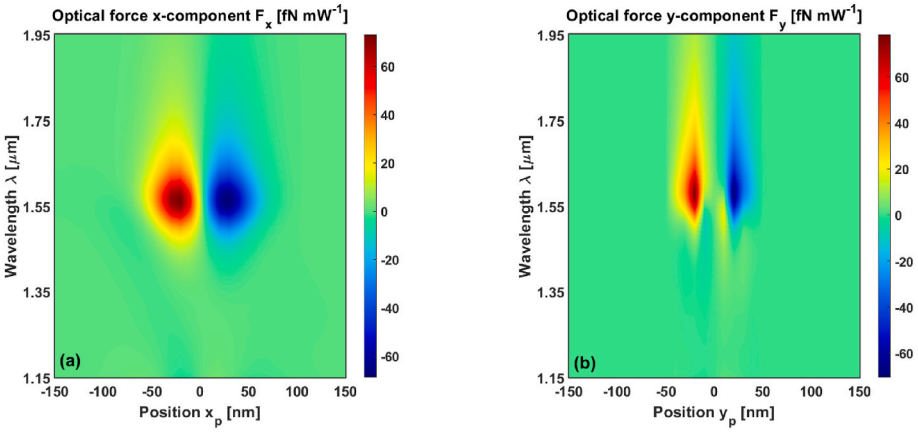

Fig. 7. (a) Optical force x-component F_x as a function of the position x_p of the nanoparticle and the wavelength λ. (b) Optical force y-component F_y as a function of the position y_p of the nanoparticle and the wavelength λ. Inner radius $r_i = 60$ nm, outer radius $r_e = 71$ nm, gap $g = 20$ nm, height $h = 15$ nm, angle $\vartheta = 90°$, nanoparticle radius $r_p = 25$ nm.

$$U(\boldsymbol{r}_0) = -\int_{-\infty}^{\boldsymbol{r}_0} \boldsymbol{F}\cdot d\boldsymbol{r} \tag{2}$$

Fig. 8(a) shows the stiffness k_x along the x-direction as a function of the nanoparticle position x_p and the wavelength λ. It is observed that the stiffness becomes negative at the equilibrium position. It is approximately equal to $k_x = -4.06$ fN mW^{-1} nm^{-1}, which ensures that the particle will move little while trapped. The calculated stiffness along the y-direction is slightly positive, $k_y = 0.76$ fN mW^{-1} nm^{-1}, as shown in Fig. 8(b).

Finally, the trapping potential U is evaluated by means of (2). It is worth stressing that, a univocal trapping potential can be defined only in absence of non-conservative force components. Since in the presented case, the nanoantenna driving the optical forces is excited thanks to the underlying dielectric waveguide, there will be a non-conservative scattering force component due to the directional propagation of the energy in the waveguide. This will result in a small difference in the calculation of the integral in (2) if the integration path is oriented along the x-direction or the y-direction. The result is shown in Fig. 9, which reports the trapping potentials U_x and U_y along the x-direction and the y-direction, respectively, both normalized to k_BT, as functions of the nanoparticle position and the wavelength λ. The resulting potential wells have a depth of approximately $U_x = -0.684 k_BT$ mW^{-1} and $U_y = -0.37 k_BT$ mW^{-1}. Consequently, an input power of $P_{in} = 27$ mW at $\lambda = 1.55$ μm is sufficient to meet the Ashkin criterion and stably trap the nanoparticle.

3. Conclusions

An integrated plasmonic near-field tweezers based on a novel nanoantenna design consisting in two gold half-ring elements has been proposed and designed. The structure exhibits a great versatility due to the high number of geometrical parameters, making it possible to tailor the resonance wavelength of the plasmonic tweezers. The trapping performance was investigated by evaluating the optical force exerted on a nanoparticle of $r_p = 25$ nm radius, along with the stiffness and the trapping potential. Simulation results have shown that stable trapping is achieved for an input power as low as $P_{in} = 27$ mW at $\lambda = 1.55$ μm, with a stiffness $k_x = -4.06$ fN mW^{-1} nm^{-1}. This input power is 10% lower than that reported in [4], where an input power $P_{in} = 30$ mW was required to trap a nanoparticle having the same radius $r_p = 25$ nm. Moreover, a slightly smaller stiffness $k_x = -3.12$ fN mW^{-1} nm^{-1} was also reported in [4], but for a nanoparticle having radius $r_p = 50$ nm. Further improvements could be obtained by: (i) adding dielectric nanorods inside the half-ring elements to mechanically filter the nanoparticles; (ii) considering a chain of multiple half-ring elements with different sizes, paving the way to wavelength-selective optical trapping.

CRediT authorship contribution statement

Mario Christian Falconi: Conceptualization, Investigation, Writing – original draft, Writing – review & editing. **Giovanni Magno:**

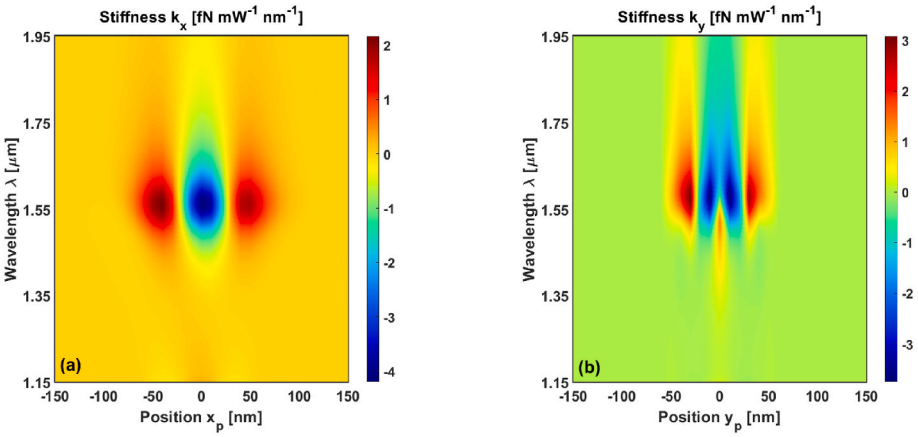

Fig. 8. (a) Stiffness k_x along the x-direction as a function of the position x_p of the nanoparticle and the wavelength λ. (b) Stiffness k_y along the y-direction as a function of the position y_p of the nanoparticle and the wavelength λ. Inner radius $r_i = 60$ nm, outer radius $r_e = 71$ nm, gap $g = 20$ nm, height $h = 15$ nm, angle $\vartheta = 90°$, nanoparticle radius $r_p = 25$ nm.

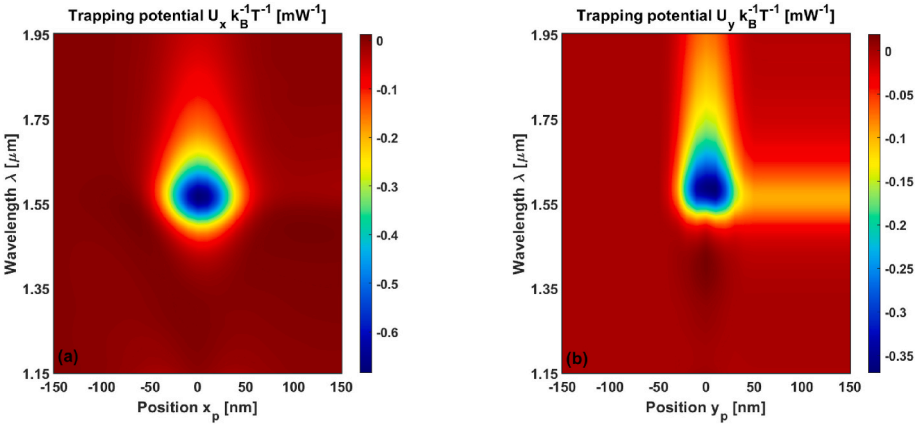

Fig. 9. (a) Trapping potential U_x, normalized to k_BT, along the x-direction as a function of the position x_p of the nanoparticle and the wavelength λ. (b) Trapping potential U_y, normalized to k_BT, along the y-direction as a function of the position y_p of the nanoparticle and the wavelength λ. Inner radius $r_i = 60$ nm, outer radius $r_e = 71$ nm, gap $g = 20$ nm, height $h = 15$ nm, angle $\vartheta = 90°$, nanoparticle radius $r_p = 25$ nm.

Resources, Writing – review & editing. **Santina Colosimo:** Validation, Investigation, Visualization. **Vy Yam:** Writing – review & editing. **Beatrice Dagens:** Supervision. **Francesco Prudenzano:** Supervision.

Declaration of competing interest

The authors declare that they have no known competing financial interests or personal relationships that could have appeared to influence the work reported in this paper.

Acknowledgements

This research has been partially developed within the projects: PON R&I 2014–2020 "AIM: Attraction and International Mobility", n. AIM1895471-3, line 1; PON R&I 2014–2020 "New Satellites Generation components – NSG" n. ARS01_01215; MIUR, PNR 2015–2020, "Agriculture Green & Digital – AGREED", n. ARS01_00254; H2020-ICT-37-2020 "Photonic Accurate and Portable Sensor Systems Exploiting Photo-Acoustic and Photo-Thermal Based Spectroscopy for Real-Time Outdoor Air Pollution Monitoring – PASSEPARTOUT" n. 101016956. GM is supported by a grant from Regione Puglia "Research for Innovation" (REFIN). REFIN is an intervention co-financed by the European Union under the POR Puglia 2014–2020, Priority Axis OT X "Investing in education, training and professional training for skills and lifelong learning" - Action 10.4 - DGR 1991/2018 - Notice 2/FSE/2020 n. 57 of May 13, 2019 (BURP n. 52 of June 16, 2019).

References

[1] K.A. Willets, R.P. Van Duyne, Localized surface plasmon resonance spectroscopy and sensing, Annu. Rev. Phys. Chem. 58 (2007) 267–297, https://doi.org/10.1146/annurev.physchem.58.032806.104607.

[2] P. Lin, H. Chu, T. Lu, P. Lee, Trapping particles using waveguide-coupled gold bowtie plasmonic tweezers, Lab Chip 14 (2014) 4647–4652, https://doi.org/10.1039/C4LC00731J.

[3] Y. Lin, P. Lee, Efficient optical trapping of nano-particle via waveguide-coupled hybrid plasmonic nano-taper, IEEE Photon. J. 11 (2019) 1–12, https://doi.org/10.1109/JPHOT.2019.2912836.

[4] A. Ecarnot, G. Magno, V. Yam, B. Dagens, Ultra-efficient nanoparticle trapping by integrated plasmonic dimers, Opt. Lett. 43 (2018) 455–458, https://doi.org/10.1364/OL.43.000455.

[5] R.-C. Jin, J.-Q. Li, L. Li, Z.-G. Dong, Y. Liu, Dual-mode subwavelength trapping by plasmonic tweezers based on V-type nanoantennas, Opt. Lett. 44 (2019) 319, https://doi.org/10.1364/ol.44.000319.

[6] Q. Jin, L. Wang, S. Yan, H. Wei, Y. Huang, Plasmonic nano-tweezer based on square nanoplate tetramers, Appl. Opt. 57 (2018) 5328, https://doi.org/10.1364/ao.57.005328.

[7] M. Samadi, S. Vasini, S. Darbari, A.A. Khorshad, S.N.S. Reihani, M.K. Moravvej-Farshi, Hexagonal arrays of gold triangles as plasmonic tweezers, Opt Express 27 (2019) 14754–14766, https://doi.org/10.1364/OE.27.014754.

[8] K. Wang, E. Schonbrun, P. Steinvurzel1, K.B. Crozier, Trapping and rotating nanoparticles using a plasmonic nano-tweezer with an integrated heat sink, Nat. Commun. 2 (2011) 1–6, https://doi.org/10.1038/ncomms1480.

[9] D. Yoo, K.L. Gurunatha, H.-K. Choi, D.A. Mohr, C.T. Ertsgaard, R. Gordon, S.-H. Oh, Low-power optical trapping of nanoparticles and proteins with resonant coaxial nanoaperture using 10 nm gap, Nano Lett. 18 (2018) 3637–3642, https://doi.org/10.1021/acs.nanolett.8b00732.

[10] T. Shoji, J. Saitoh, N. Kitamura, F. Nagasawa, K. Murakoshi, H. Yamauchi, S. Ito, H. Miyasaka, H. Ishihara, Y. Tsuboi, Permanent fixing or reversible trapping and release of DNA micropatterns on a gold nanostructure using continuous-wave or femtosecond-pulsed near-infrared laser light, J. Am. Chem. Soc. 135 (2013) 6643–6648, https://doi.org/10.1021/ja401657j.

[11] J.J. Baker, F. Crivellari, Z. Gagnon, M.J. Betenbaugh, Microfluidic bubbler facilitates near complete mass transfer for sustainable multiphase and microbial processing, Biotechnol. Bioeng. 113 (2016) 1924–1933, https://doi.org/10.1002/bit.25972.

[12] K. Ying, M.K.H. Al-Mashhadani, J.O. Hanotu, D.J. Gilmour, W.B. Zimmerman, Enhanced mass transfer in microbubble driven airlift bioreactor for microalgal culture, Eng. Times 5 (2013) 735–743, https://doi.org/10.4236/eng.2013.59088.

[13] A. Ashkin, J.M. Dziedzic, J.E. Bjorkholm, S. Chu, Observation of a single-beam gradient force optical trap for dielectric particles, Opt. Lett. 11 (1986) 288–290, https://doi.org/10.1364/OL.11.000288.

[14] G. Magno, A. Ecarnot, C. Pin, V. Yam, P. Gogol, R. Mégy, B. Cluzel, B. Dagens, Integrated plasmonic nanotweezers for nanoparticle manipulation, Opt. Lett. 41 (2016) 3679–3682, https://doi.org/10.1364/OL.41.003679.

[15] Q. Hao, H. Huang, X. Fan, Y. Yin, J. Wang, W. Li, T. Qiu, L. Ma, P.K. Chu, O. G. Schmidt, Controlled patterning of plasmonic dimers by using an ultrathin nanoporous alumina membrane as a shadow mask, ACS Appl. Mater. Interfaces 9 (2017) 36199–36205, https://doi.org/10.1021/acsami.7b11428.

[16] C. Ge, Z. Wu, J. Bai, L. Gong, Effect of nanoscale roughness on optical trapping properties of surface plasmon polaritons exerted on nanoparticle, J. Quant. Spectrosc. Radiat. Transf. 219 (2018) 339–349, https://doi.org/10.1016/j.jqsrt.2018.08.020.

[17] D.G. Kotsifaki, S.N. Chormaic, Plasmonic optical tweezers based on nanostructures: fundamentals, advances and prospects, Nanophotonics 8 (2019) 1227–1245, https://doi.org/10.1515/nanoph-2019-0151.